

Deciphering the Effect of Traps on the Electronic Charge Transport Properties of Methylammonium Lead Tribromide Perovskites

Artem Musiienko^{1*}, Jindřich Pipek¹, Petr Praus¹, Mykola Brynza¹, Eduard Belas¹, Bogdan Dryzhakov², Mao-Hua Du³, Mahshid Ahmadi^{2**}, Roman Grill¹

¹*Charles University, Faculty of Mathematics and Physics, Institute of Physics, Ke Karlovu 5, CZ-121 16, Prague 2, Czech Republic*

²*Joint Institute for Advanced Materials, Department of Materials Science and Engineering, University of Tennessee, Knoxville, TN 37996, USA*

³*Oak Ridge National Laboratory, Materials Science and Technology Division, Oak Ridge, USA*

Corresponding authors emails:

* musiienko@karlov.mff.cuni.cz,

** mahmadi3@utk.edu

Abstract:

Organometallic halide perovskites (OMHPs) have gained a remarkable development as highly efficient optoelectronic materials for variety of applications. Several studies indicated the critical role of defects on the performance of OMHP devices. Yet, the parameters of defects and their interplay with free charge carriers remains unclear. In this study we explore the dynamics of free holes in methylammonium lead tribromide (MAPbBr₃) single crystals using time of flight (ToF) current spectroscopy. By combining the current waveform (CWF) ToF spectroscopy and Monte Carlo (MC) simulation, three energy states were detected in the band gap of MAPbBr₃ and the trapping-detrapping rates of free holes in the range of few μ s up to hundreds of μ s were calculated for the first time. Contrary to the previous studies a strong detrapping activity was revealed. It was shown that these traps have a significant impact on the transport properties of MAPbBr₃ single crystal device including drift mobility and mobility-lifetime product. To demonstrate the delaying activity of traps we developed a new model of the effective mobility valid for the case of multiple traps in a material. Our results provide a new insight on charge transport properties of OMHP semiconductors which is required for further development of optoelectronic devices.

Introduction

Despite impressive progress in commercialization of Si photovoltaics (PVs) in the last decade, the Si-based single-junction PV efficiency has been increased only a few percents approaching the theoretical limit of 29%^[1]. Therefore, current research and production trends aim at increasing the efficiency by searching alternative materials, new tandem PV designs, and reducing the cost of industrial modules. Recently, the arising of inexpensive organometallic halide perovskite (OMHP) semiconductors with unique light conversion efficiency and charge transport properties led to rapid development of a new generation of solar cells. The efficiency of such solar cells significantly increased from 3.8% in the year 2009 up to 23.7%^[2,3] in 2019. Another great advantage of OMHP semiconductors is the fabrication capability on flexible substrates^[4-7], which offers an additional opportunity for the development of portable power sources^[8] and new PV architectures^[9,10]. Among wide compositional range of OMHPs, methylammonium lead tribromide perovskite (MAPbBr₃) has attracted a great interest for application in tandem PVs^[11-16], as well as in light-emitting diodes^[17,18], lasers^[19], photodetectors^[19,20] and high energy radiation sensors^[21-24].

One of the most critical factors in the performance of multifunctional OMHP devices is the presence of trapping centers resulting in the loss of charge collection efficiency in a solar cell or detector performance. Trapping centers in a semiconductor lattice lead to the formation of energy levels^[25-28] in the band gap. These energy states affect the relaxation dynamics of free carriers by trapping processes and therefore, detrimentally influence the free charge transport properties such as lifetime and drift mobility. The detection and characterization of such traps and their associated relaxation dynamics are highly challenging due to the dominant non-radiative nature of such energy transitions in any types of semiconductors, restraining their investigation by photoluminescence spectroscopies^[29-31]. Other techniques such as thermal emission is limited by the low activation energy of shallow levels and the presence of several phase transitions in OMHPs^[32,33] preventing them from adequate cooling to reveal the trapping parameters of defects.

Recently, by combining current waveform Time of Flight (CW ToF) and photo-Hall effect spectroscopy (PHES) we revealed deep levels and their relative positions in the bandgap of MAPbBr₃ single-crystal device^[27]. Other research groups observed similar deep energy transitions^[34,35]. In addition, theoretical calculations revealed multiple shallow levels in OMHPs^[36-41]. Yet, the trapping parameters – trapping and detrapping time – of these levels and the interplay of free charge carriers with these energy levels have not been shown experimentally.

The primary aim of this study is to uncover the effect of traps on charge transport dynamics in MAPbBr₃ single crystal devices using ToF current spectroscopy. The ToF current spectroscopy is based on photo-generated charge carriers drifting through the sample under an applied bias. More explanation can be found in our previous studies^[27,42,43]. Generally, traps in a material affect the charge cloud and as a result, the measured current waveforms (CWFs). Thus, CWF consists valuable information of free carrier relaxation including trapping and detrapping from the states in the bandgap. To model the experimental results of ToF spectroscopy, and to decipher the effect of trapping and detrapping of holes from each defect state, we first solve charge transport equations by one dimensional (1D) MC^[44] simulation. In this simulation, each MC particle (hole in here) exists either in a free state drifting with a velocity of $\mu_h E(x)$ in the valence band (where μ_h is the drift mobility and $E(x)$ is the applied electric field) or trapped in one of the states in the band gap. In this way, the simulated trapping-detrapping history of charge carriers by the MC method will enable a novel insight into the free carrier dynamics and charge transport across the bulk of MAPbBr₃ single crystal. Using MC simulation we develop a charge transport model, including non-radiative energy transitions associated with traps. We simulate how the trapping and detrapping of photogenerated charge carriers from traps limit the free carrier drift in MAPbBr₃ single crystal device at different biases relevant to the operation of optoelectronic devices. The proposed model is verified using ToF bias dependence.

Next, it is known that the predicted multiple energy levels in the band gap of OMHP complicate the dynamics of charge transport beyond the classical model of trap controlled mobility^[45,46]. Such a model also known as effective mobility considers a semiconductor with a single trap delaying free carriers. Therefore, a new approach is necessary to unambiguously describe the dynamics of free charge carrier transport in this class of semiconductors. To do this, we first investigate the delay of charge carriers and identify the effective transit time of the delayed charge cloud by MC simulation. We then reassess the definition of the effective mobility (μ_h^{eff}) according to the effective transit time associated with the center of the delayed charge cloud. Such approach allows us to study charge transport properties in any other semiconductors with any number of active traps. Finally, we analyze the effect of traps on the effective mobility of holes and its relationship with the electric field and thickness of OMHP devices.

In addition, to demonstrate the effect of traps on the performance of MAPbBr₃ single crystal device we explore the effect of traps activity on the lifetime-mobility product. Understanding the

impact of traps on charge transport properties is necessary to control the traps and to further improve the performance of OMHP devices.

Results and discussion

Charge Transport Dynamics in Single crystals of MAPbBr₃ perovskite

The temporal dynamics of free carriers is considered as the most crucial characteristic of material defining efficiency of a semiconductor device. This temporal dynamics, given by Equation (1), is mainly affected by energy states in the band gap.

$$\frac{dp}{dt} = \sum_i \left(-\frac{p}{\tau_{Ti}} + \frac{p_{Ti}}{\tau_{Di}} \right) \quad (1)$$

where the defect influence on free hole concentration (p) is described by the specific trapping (τ_{Ti}) and detrapping times (τ_{Di}) of the i -th level; and p_{Ti} is the concentration of the holes trapped in the i -th level. Depending on the trapping and detrapping times, defects can induce short-term and long-term trapping of free carriers. The presence of trap supporting fast trapping-detrapping processes in a material leads to delay of the free carrier drift and consequently reduce the drift mobility. Theoretically, the long-term trapping is commonly associated with carrier lifetime (τ_{life}). However, in reality a trapping center releases the trapped carrier after τ_{Di} , and the detrapped free carriers continue moving through a semiconductor. This controversy leads to an underestimation of the transport features and the charge collection properties in the semiconductor device. By probing ToF signal in MAPbBr₃ single crystal device we found reliable holes signal in the CWFs ToF measurements, but the electron signal could not be revealed (**Figure 1a**). Therefore, here we only study free hole transport. By studying transit time (T_R) of the CWFs ToF i.e. the time required for the hole to transit through a semiconductor and relaxation dynamics before and after T_R we can reveal the information of holes interaction with defects during drift across the semiconductor.

To demonstrate free holes interaction with traps in MAPbBr₃ single crystal device we study the ToF current induced by free photoexcited holes collected by 100 V bias. The anode immediately collects the electron cloud, and only free holes drifting through the bulk of MAPbBr₃ towards the cathode induce ToF signal. As shown in **Figure 1a** holes drift in the material reveal a sophisticated relaxation dynamics: two-exponential decaying regions before transit time (T_R), 32 μ s and a long current tail after T_R . The sharp transit time of 32 μ s indicates the insignificant impact of free holes

recombination because a fraction of the charge cloud reached the cathode and produced transit time banding of CWF. The long T_R indicates the long lifetime of holes ($\tau_{\text{life}} > T_R$) in MAPbBr₃ single crystal device, but highlights the relatively low free hole mobility because of long transit time.

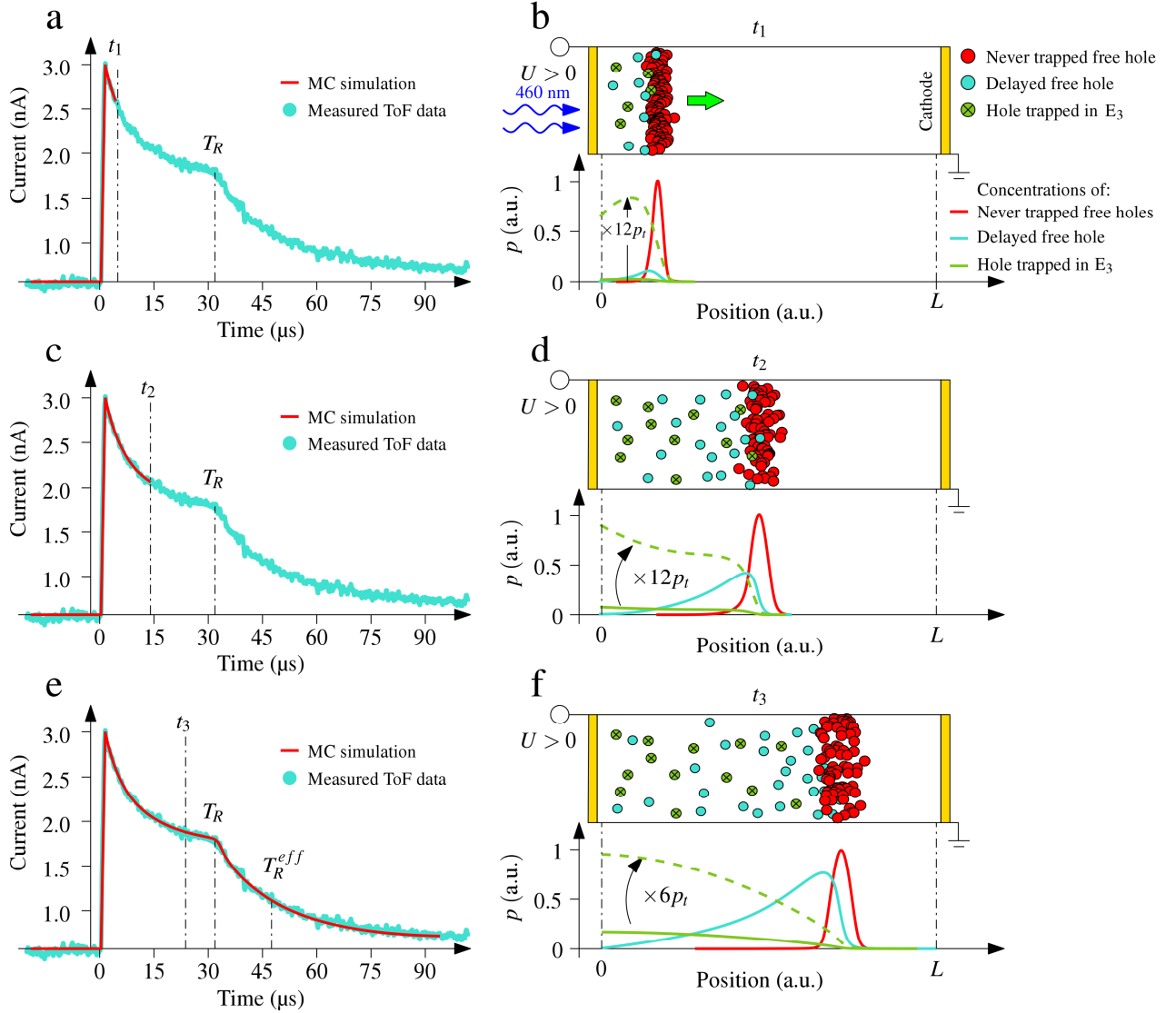


Figure 1. a), c), and e) ToF CWF measured at 100 V. The red curve shows the best MC simulation fit with three energy levels at different times $t_1 = 6$, $t_2 = 14$, and $t_3 = 23$ μs respectively. b), d), and f) the top panels demonstrate the time evolution of free charge cloud (subdivided according to their trapping-detrapping history) during the drift process at t_1 , t_2 , and t_3 , respectively. The bottom panels show the respective normalized concentrations of never trapped holes, trapped and delayed holes in the material.

To explore the complex charge dynamics and to assess transport parameters of MAPbBr₃ we applied MC simulation in combination with least square regression analysis. The details of the MC simulation (Figure S1 and Equations S1-S6) and the fitting method are shown in supplementary materials (Figure S2 and Table S1). The red line in Figure 1a, c, and e represent the MC transport model with minimum deviation from the ToF spectra. This MC model – with parameters summarized in Table 1– reveals three traps affecting the hole transport. According to the simulated MC transport model (**Figure 2**) two energy levels E₁ and E₂ support fast trapping of free holes with nearly same trapping time of 23 μs and 24 μs. These levels shortly release trapped holes back to the valence band with detrapping rates of 3 μs and 14 μs, respectively. The trap level, E₃, supports the long-lasting carrier trapping with a trapping time of 90 μs. This energy level shows a relatively slow ($\tau_{D3} > T_R$) holes detrapping time of 120 μs.

Table 1 Charge transport parameters of single-crystal MAPbBr₃ found from the combination of ToF and MC simulation

Energy level	Trapping time (μs)	Detrapping time (μs)	Effective Mobility* (cm ² V ⁻¹ s ⁻¹)
E ₁	23	3	11.0
E ₂	24	14	7.8
E ₃	90	120	5.3

*The calculated effective mobility is given for the case of a single trap in MAPbBr₃.

To study the effect of traps on charge transport, it is convenient to separate the free carrier profiles from carrier trapping and detrapping phenomena. Using MC simulation, we divide the free holes into three groups: never trapped holes (holes which previously did not interact with any trap), delayed holes (holes at least once detrapped by any trap), and long-term trapped holes (holes trapped by level E₃). Figures 1b, d, and f represent detail evolution of free holes cloud drifting at different times ($t_1 = 6 \mu\text{s}$, $t_2 = 14 \mu\text{s}$, and $t_3 = 23 \mu\text{s}$) demonstrating the effect of traps on the charge cloud in MAPbBr₃ single crystal device at 100 V. Clearly, E₁ and E₂ traps decelerate free holes by relatively fast trapping-detrapping process and then the fraction of delayed holes increases with time. As can be seen in the bottom panel of Figure 1f when the charge cloud reaches the collecting electrode the delayed holes concentration is comparable with the concentration of never trapped holes. Thus, the detrapped carriers create an extended profile of delayed holes which deviate from the total charge cloud in the Gaussian distribution (see blue and red lines in Figure 1f).

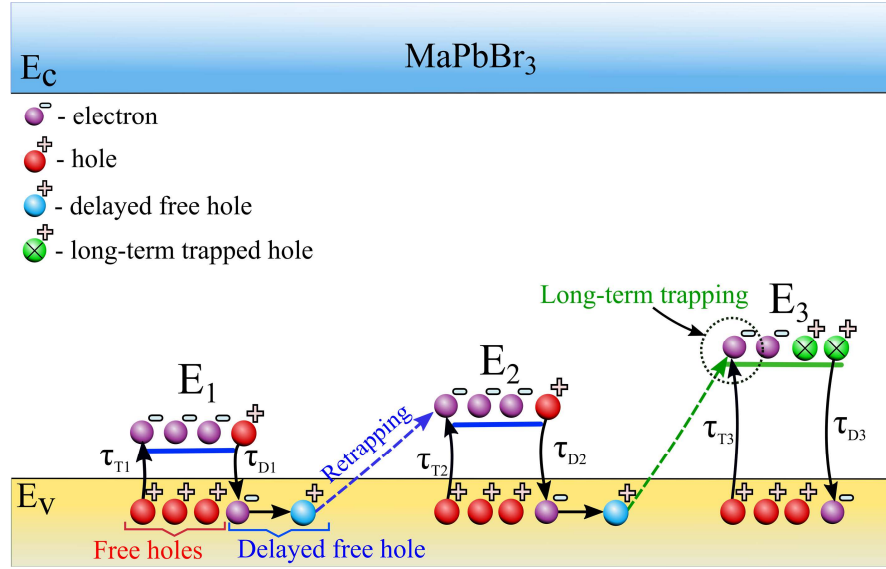


Figure 2. Charge transport model of single crystal MAPbBr₃. Upward and downward arrows illustrate energy transitions estimated by ToF and MC simulation. Table 1 summarizes the parameters of these transitions.

In contrary to the fast trapping-detrapping dynamics, the trap E₃ support long-term trapping of holes which remain trapped in this defect (*p_i*) during the whole drifting process (see Figure 1f). Considering the center of total free holes cloud using MC simulation we can evaluate the effective transit time, $T_R^{eff} = 48 \mu\text{s}$ (see Figure 1e) which express the average delaying of the holes cloud by traps; meanwhile $T_R = 32 \mu\text{s}$ reflects the transit time of only the fraction of free carriers associated with the never trapped holes.

Here, we revealed the presence of traps, their parameters, and their role in delaying free holes at 100 V. It is expected that the levels E₁, E₂, and E₃ are located near the valence band as they have a direct influence on free holes transport in MAPbBr₃.

Verification of the charge transport model and uniform electric field profile

It is well established that the drift velocity (v_{dr}) of charge carriers conducted by a uniform electric field (E) is directly proportional to the electric field and the free carrier mobility. Therefore, free carriers drifted by a lower bias need longer time to be collected by the electrode (for details see Figure S2b and Equation S7 in supplementary materials). To verify the simulated MC transport model and to study the effect of electric field on transit time and hole trapping dynamics, CWF ToF measurements were performed at different biases (**Figure 3a**). The MC simulation (based on parameters in Table 1) agrees with experimental bias dependence of CWF and follows the main trends of ToF results, including the sharp current decrease at the beginning of CWF and the long tail after T_R . The effect of trap E_3 is even more evident at lower biases between 20 to 80 V. As can be seen in Figure 3b, all experimental CWFs, as well as MC simulation, follow the same trend of a single trap with slow detrapping (level E_3) in charge transit region, $t < T_R$. The good agreement of the simulated model at all biases further confirms the reliability of MC simulation and the proposed explanation of charge transport dynamics.

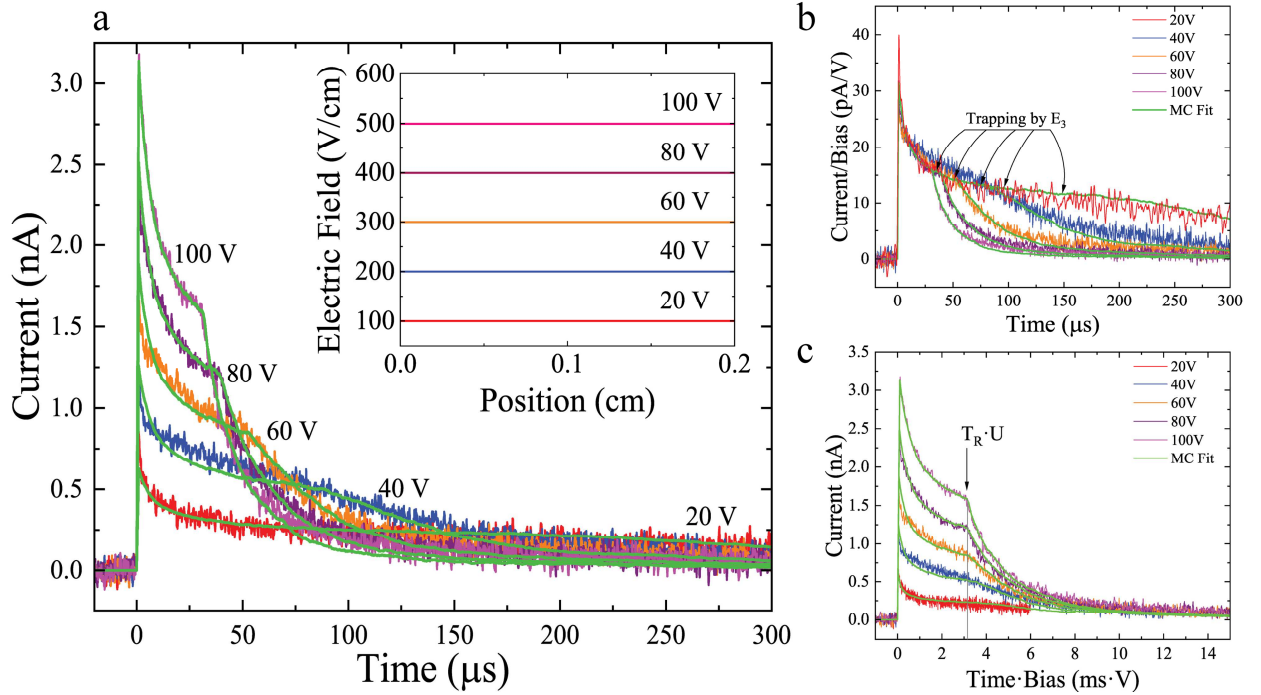


Figure 3. a) Bias dependence of CWFs. The green curves represent the simulated MC fit. The inset shows electric field profiles between two electrodes. b) Normalized CWFs at different biases. c) CWFs dependence on normalized time according to Equation 2.

In addition to short and long-term charge trapping, defects can induce electric field distortion by creating a depletion region near the metallic electrode^[42]. Several studies demonstrated the presence of mobile defects in OMHPs and discussed that the collection of these low mobile species at the interface could lead to deformation of the electric field profile^[47]. To suppress the possible formation of the space charge in the sample during ToF experiment, we use 1 ms short voltage pulse and synchronized it with 100 ns light pulse (see details in supplementary materials and method section). It should be noted that the drift of photo-induced carriers through the material can also result in electric field distortion. Considering the low carrier concentration of $\sim 10^6 \text{ cm}^{-3}$ calculated from Figure 3a, an electric field distortion of 0.6 Vcm^{-1} is obtained (see details in supplementary materials Equation S8). Therefore, the effect of free charge carriers on the electric field distortion is negligible.

Despite low holes concentration and pulsed bias indicating a uniform electric field, CWFs at different biases can be used to verify the electric field profile and the presence of the space charges. According to Equation 2 the measured ToF CWFs at different biases U in a semiconductor with negligible space charge supports the condition where the transit time of never-trapped charge cloud between two electrodes multiplied by applied bias is constant for any bias.

$$T_R(U) \cdot U = \text{const} \quad (2)$$

while, the presence of a non-negligible space charge leads to deviation from this equation. According to CWFs ToF and MC shown in Figure 3c, all CWFs have the same $T_R(U) \cdot U$ product which confirms the uniform distribution of electric field in MAPbBr₃ single crystal device.

Charge distribution in MAPbBr₃ induced by energy states at different biases

In the previous section we showed that fast and slow trapping-detrapping processes induced by three energy states in the band-gap affect the charge dynamics in MAPbBr₃. To further explore the influence of each energy level on the charge transport with different drift velocities at 100, 20, and 1 V, the time evolution of charge cloud is explored using MC simulation and ToF CWF (**Figure 4**). Interestingly, we found that the relaxation dynamics of free holes changes with bias (Figure 4a, c, and e). These changes can be attributed to the interplay of traps with free holes. It was shown that the number of trapping-detrapping events induced by traps increases at lower electric field. This is because the charge cloud needs more time to drift across the material and as a result higher

possibility to interact with defects. As can be seen in Figure 4b, d, and f at lower biases the fraction of delayed holes is higher and delay of the total holes cloud is more significant.

As can be seen in Figure 4a, c, d the interplay of free holes with traps follows four regions. After the light pulse generates holes, they start to drift in the bulk of the material. Thus, all traps actively capture the free holes leading to an increase in the occupation of all defects and consequently decrease of the free holes concentration in region **(i)**. The charge trapping induced by traps E_1 and E_2 dominates in the region (i) with faster trapping times. The trap E_1 first reach to a saturation point (steady-state condition in which the trapping and detrapping rate are equal) due to faster detrapping time of this trap ($\tau_{D1} > \tau_{D2} > \tau_{D3}$). Then the holes detrapped from E_1 are retrapped by traps E_2 and E_3 . Usually in the material with a single trap, the occupation of trap does not change after steady state condition. But due to three traps in MAPbBr₃ the occupation of trap E_1 starts to decrease after saturation point as a result of trapping induced by traps E_2 and E_3 . We note that the cross retrapping processes of delayed free holes can play an important role in an additional delay of the charge cloud.

Similar to trap E_1 , trap E_2 reaches a saturation point at region **(ii)**. When traps E_1 and E_2 both attain steady-state conditions, they do not capture additional free holes; therefore the trap E_3 further dominates the free carriers trapping which leads to an exponential decay of free holes in the region (ii) with the time constant τ_{T3} . At the time T_R the never trapped holes (holes which did not interact with traps) reach the cathode in region **(iii)**. Since a fraction of holes were collected at the electrode, the occupation of all traps decreases after the transit time. As shown in bottom panels of Figure 4b, d, and f, due to the presence of several traps supporting trapping-detrapping events and cross retrapping in MAPbBr₃, a significant concentration of delayed holes reaches electrode after T_R . Here, delaying of the charge cloud results in prolongation of the effective transit time, T_R^{eff} , at lower biases in comparison with T_R .

Finally, at biases lower than 1 V ($E < 5 \text{ Vcm}^{-1}$) in region **(iii)**, all traps reach a steady-state condition after processes considered in the regions (i) and (ii); therefore, the occupation of the traps and free holes is not changing with time. Due to long T_R ($T_R > \tau_{D3}$) defect E_3 also participate in the holes detrapping in the region (iii). The steady-state regime in the time region (iii), is qualitatively similar to the steady-state photoconductivity or solar cell operation regime. Indeed, the continuous illumination utilized in PV devices leads to redistribution of free charges, and a significant fraction of the photo-generated carriers remains trapped in defect E_3 .

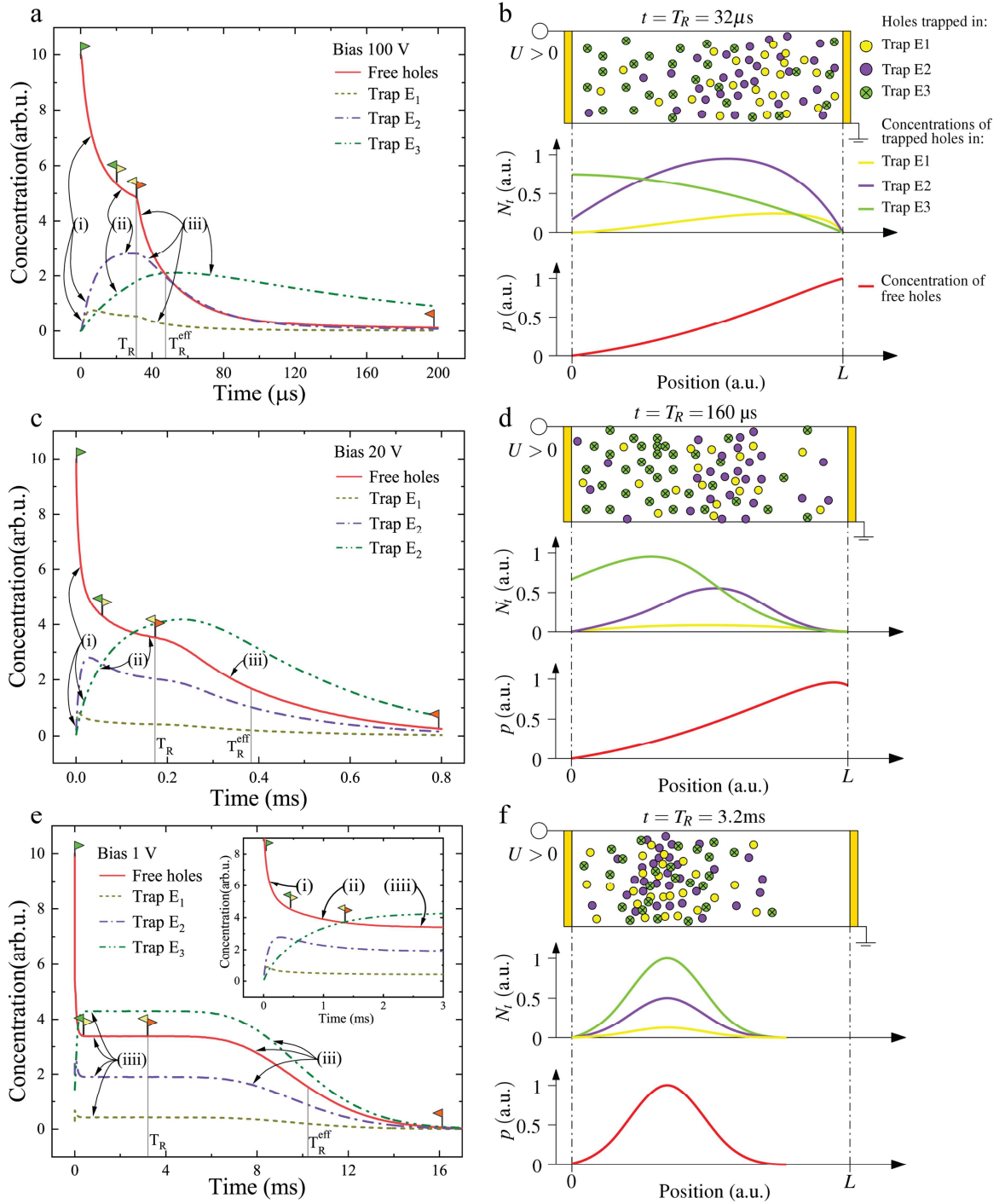


Figure 4. The evolution of free holes concentration and occupation of energy states in MAPbBr₃ at 100 V a)-b), 20 V c)-d), and 1 V e)-f). Figures 4a), c), and e) represent the temporal evolution of free carriers and traps occupation. Flag indicators separate the regions (i)-(iii) with different relaxation

dynamics characters. Figures 4b), d), and f) show the simulated spatial visualization of traps (top panel), the distribution of traps occupation (middle panel), and profile of charge cloud in MAPbBr₃ at different biases (bottom panel).

Note that at low electric field (Figure 4f), the charge cloud does not reach halfway to the bulk – in the transit time corresponding to the never trapped holes – due to delaying activity of traps. This example explicitly shows the highly detrimental influence of traps on the charge drift in OMHP devices. Besides decreasing the charge collection efficiency, the trapped carriers also contribute to the memory effect and the variation of device transport parameters based on the rate of scanning (up to few ms) and illumination intensity.

Delaying effect of traps on the charge transport

Using ToF combined with MC simulation we demonstrated that activity of traps leads to a noticeable delay of the charge cloud. The effective mobility, μ_h^{eff} , can qualitatively describe this delaying process. Therefore, the conventional model^[45,48] considering a single trap in the material can be modified for the case of multiple traps activity (see Equations S9-S16 in supplementary materials). The following equation expresses the influence of shallow levels on average carrier velocity in a trap-controlled mobility drift regime

$$\mu_h^{eff} = \mu_h \frac{1}{1 + \sum_i \frac{\tau_{Di}}{\tau_{Ti}}} \quad (3)$$

where μ_h^{eff} is the effective mobility of holes. On the other hand, this definition is only valid when all traps reach a saturation point i.e. the condition at low biases < 1 V ($E < 5$ Vcm⁻¹). Therefore, a new definition is necessary to describe μ_h^{eff} at higher biases as well.

To modify the effective mobility, μ_h^{eff} , we track the center of the charge cloud drifting in the semiconductor with multiple traps. Indeed, the MC simulation allows us to determine the effective transit time, T_R^{eff} , of the total charge cloud and to calculate corresponding effective mobility. The effective mobility can be defined by the following equation,

$$\mu_h^{eff} = \mu_h \frac{T_R}{T_R^{eff}} \quad (4)$$

where the effective transit time, T_R^{eff} , describes how the traps delay the drift of free charge cloud.

Note that in the case of trap activity, the charge cloud undergoes significant deformation (Figure 4b, d, and e) and the drift mobility (μ_h) cannot be found only by ToF measurements without considering the delaying effect of traps. The value of μ_h unaffected by shallow traps can be determined by considering the trapped and detrapped carriers in the MC simulation.

To analyze the influence of each level on free carrier drift and the effective mobility, we show the MC dependence of μ_h^{eff} on the electric field at different MAPbBr₃ thickness (**Figure 5**). We first consider the effective mobility dependence at high electric fields where there is no influence of traps. When a high electric field is applied to the sample the electrode rapidly collects the holes charge cloud excluding interaction with traps in the material. Therefore, the effective mobility converges to the drift mobility unaffected by traps (i.e. 12.4 cm²V⁻¹s⁻¹). The effective mobility further decreases with decreasing electric field due to the interaction of the free charge cloud with traps. The traps, E₁ and E₂, support trapping-detrapping events with the single trap effective mobilities (μ_{eff}^{E1} and μ_{eff}^{E2}) of 11.0 cm²V⁻¹s⁻¹ and 7.8 cm²V⁻¹s⁻¹, respectively (see Equation 3 and Table 1). These two traps induce the primary reduction trend of $\mu_h^{eff}(E)$. After μ_h^{eff} reaches the μ_{eff}^{E2} , it continues to decrease with decreasing electric field due to the cross retrapping of detrapped holes assisted by traps E₁ and E₂. Indeed, as was previously demonstrated in Figure 4a, c, d, trap E₁ first reaches to the steady-state point and after $t = \tau_{DI} = 3 \mu\text{s}$ this level actively detrappes holes. The detrapped carriers from defect E₁ are further trapped and detrapped by trap E₂. The interplay between detrapped holes and fast traps (E₁ and E₂) lead to the decrease of effective mobility up to 7.2 cm²V⁻¹s⁻¹ (μ_{eff}^{E1+E2}) below the value of effective mobility induced by single level E₂ (7.8 cm²V⁻¹s⁻¹).

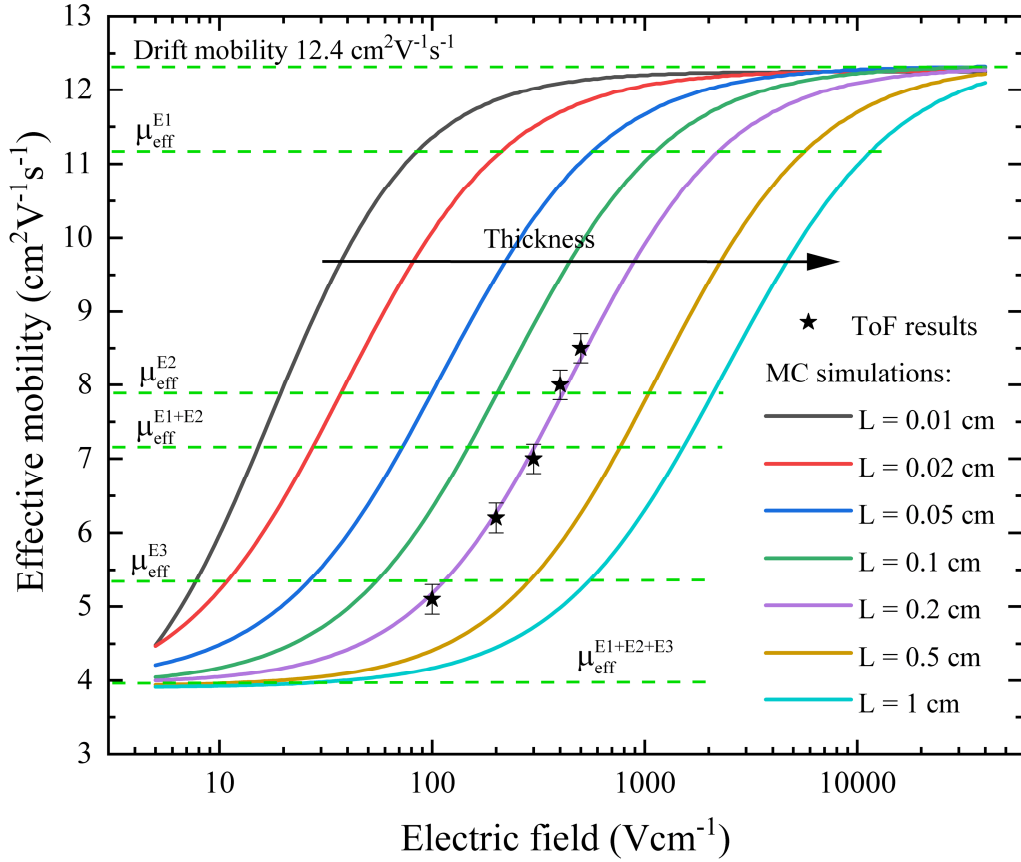


Figure 5. The MC dependence of effective mobility on electric field. Parameter L represents the thickness of the material. Stars show ToF experimental results ($L=0.2$ cm) of effective mobility.

At low electric field (for example, 300 Vcm^{-1} and 0.2 cm device thickness) the T_R of the charge cloud is higher than τ_{D3} , therefore trap E_3 participates in the delay of the holes cloud, and further decreases the effective mobility. After μ_h^{eff} reaches the $\mu_{eff}^{E3} = 5.3 \text{ cm}^2\text{V}^{-1}\text{s}^{-1}$, it continues to decrease μ_{eff}^{E3} due to interplay of all three levels with delayed holes and cross retrapping processes. Notably, the value of μ_h^{eff} saturates to the value of $4.0 \text{ cm}^2\text{V}^{-1}\text{s}^{-1}$ ($\mu_{eff}^{E1+E2+E3}$) which is the same value given by classical equation represented by Equation 3. This clearly demonstrates that the proposed model of effective mobility correctly describes delaying of the charge cloud starting from trap controlled mobility regime up to the point where traps do not influence charge transport in a MAPbBr₃ single crystal device.

To study thickness dependence of effective mobility, we applied MC simulation. As shown in Figure 5 the variation in the thickness of MAPbBr₃ device at a constant electric field varies in the transit time of the drifting charge cloud (according to Equation S7) and shifts the $\mu_h^{eff}(E)$ dependence. The $\mu_h^{eff}(E)$ rapidly converges to the drift mobility in thin devices as the free holes quickly reach the collecting electrode reducing their interaction with traps. In contrast, a large number of trapping-detrapping events appear in thick samples where the charge cloud attains more time to interact with traps. Therefore, μ_h^{eff} slowly converges to the μ_h in thick samples and has the lower absolute value at the same electric fields in the thin devices. Our results demonstrate that MAPbBr₃ thickness has a significant impact on free charge collection efficiency in optoelectronic devices.

Analysis of drift mobility by ToF and mobility-lifetime product ($\mu\tau$) in MAPbBr₃

Multiple ToF based techniques in both organic and inorganic semiconductors^[21,27,37,49,50] use the inflection (trap free approach^[51]) or intersection (dispersive photocurrent^[52]) points between transit and tail region of CWF (see details in Figure S4, supplementary materials) to evaluate the drift mobility. To demonstrate the possible errors in the determination of the drift mobility here, we compare the values of drift mobility calculated by MC simulation and by the standard methods (**Figure 6a**). The hole mobilities found from inflection (μ_{inf}) and intersection (μ_{inter}) transit times show notable deviation (up to 7.8 cm²V⁻¹s⁻¹ at 100 Vcm⁻¹) from the drift mobility in the MC simulation. The deviation increases at low biases which agrees with MC simulation. Note that MC simulation predicted a larger number of trapping-detrapping events induced by traps and more significant deformation of the holes cloud at lower biases. Thus, the deformed charge cloud leads to an incorrect treatment of ToF results by simplified approaches which does not include the effect of traps on the deformation of the charge cloud.

Clearly, the interplay between free charge carriers and traps can affect on the charge collection properties or mobility lifetime product, $\mu\tau$. Using ToF spectra and MC simulation fitted by Hecht equation, we study the $\mu\tau$ in MAPbBr₃ single crystal device, (**Figure 6b**). Due to free holes delay by traps the $\mu\tau$ shows a strong dependence (from 10⁻¹ cm²V⁻¹ up to 10⁻⁴ cm²V⁻¹) on the collection time needed to resolve photon or high energy radiation events. The detrimental influence of traps can be controlled by eliminating traps particularly trap E₃ or by decreasing their concentration as shown by MC simulation (**Figure 6b**). The trapping time of 90 μ s from level E₃, is in

agreement with our previous calculation of lifetime of free holes in MAPbBr₃^[27]. The longer detrapping time of 120 μs from this defect can compete with the transit time of free charge cloud and typical charge collection time of classical inorganic semiconductors (typically < 200 μs^[53,54]). Such a low trapping time of free holes highlights the advanced transport properties of MAPbBr₃ devices. Considering the collection of free holes in 200 μs, MC simulation in combination with ToF result in $\mu\tau$ of 10⁻³ in MAPbBr₃ which is competitive with the best inorganic detector and semiconductor materials such as CdZnTe, GaAs, and others^[42]. However, the interplay of free charge carriers with traps has a detrimental effect on the performance of OMHP detectors due to decreased effective drift mobility and long-term trapping. In addition, the delaying activity of traps inevitably reduce the resolution of OMHP detectors. While in OMHP solar cells, the traps can be filled during the illumination and screen the internal electric field. Similarly, the trapping-detrapping activity decreases the effective mobility which can consequently lead to instability of photo-voltage (after light is switch on/off) and cause a memory effect (hysteresis). Furthermore, the trap E₃ can enhance charge carrier recombination resulting in reduced V_{OC} in OMHP solar cells. These traps can be removed by materials processing such as growth parameters, doping, or purification. For example, recently it was shown that combining Cs and Rb in quadruple cation (Rb-Cs-FA-MA) perovskite mixtures increases the value of effective mobility and decreases the trap density, resulting in solar cells with the highest stabilized power efficiency^[55].

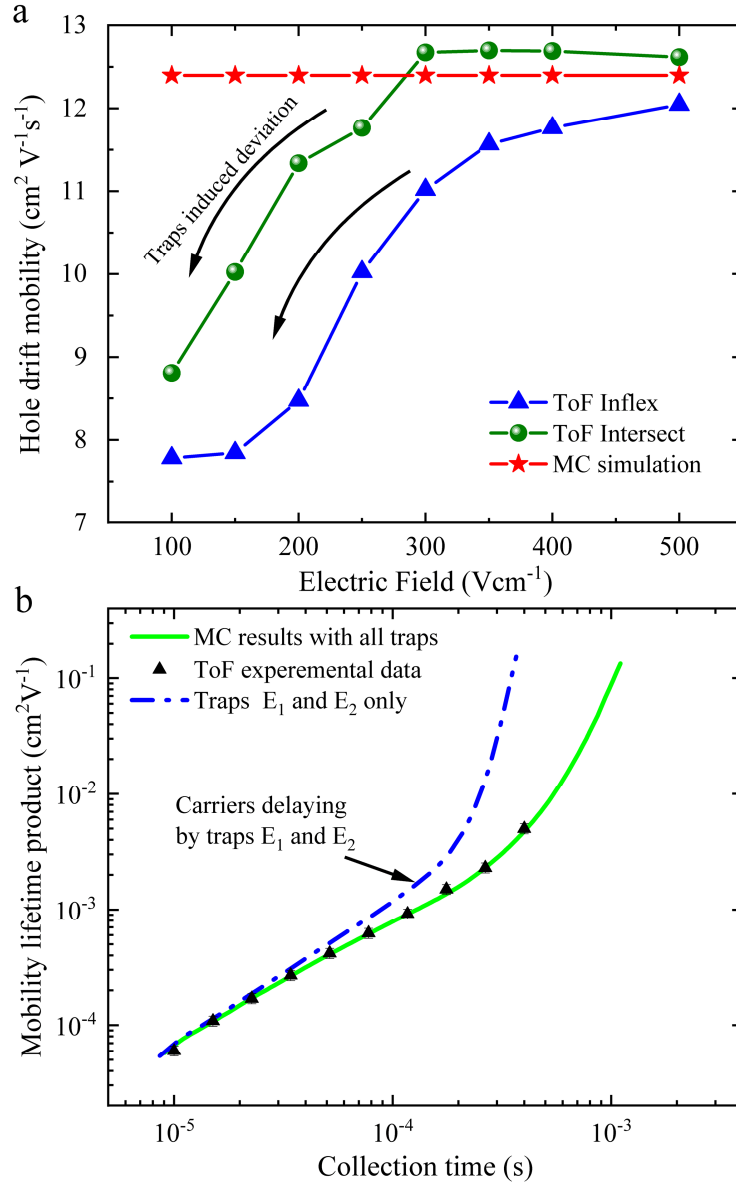


Figure 6. a) Holes drift mobility found by different approaches as a function of applied electric field according to data in Fig. R2 and MC simulation. b) Mobility-lifetime product as a function of collection time.

Conclusion

By combining Time of Flight current spectroscopy and Monte Carlo simulation, we have provided a novel insight and detail information on the dynamics of free charge carriers in MAPbBr₃ single crystal devices. We have demonstrated a strong trapping activity in MAPbBr₃ perovskite single crystal associated with three defects with trapping rates of τ_{T1} (23 μs), τ_{T2} (24 μs), and τ_{T3} (90

μ s). The complex charge transport properties of MAPbBr₃ was explained by fast detrapping rates of 3, 14, and 120 μ s from the three discovered traps, respectively. Our results revealed that traps have a significant impact on free charge transport and collection efficiency in MAPbBr₃ perovskite. It was resolved that the traps E₁ and E₂ act as shallow levels with short-term trapping-detrapping characters. While the trap E₃ acts as a deep level supporting the long- trapping of free holes.

To describe the delaying effect of traps on the charge transport properties of MAPbBr₃ single crystal peovskite a new model was proposed for the effective mobility, μ_h^{eff} . It was shown that by decreasing electric field μ_h^{eff} decreases from the drift hole mobility (12.4 cm²V⁻¹s⁻¹) down to the effective mobility calculated from the standard theory (4 cm²V⁻¹s⁻¹). This finding suggests that besides the trapping-detrapping events from defects, the intercross retrapping of the delayed holes play a significant role in the delaying of the total hole cloud. By applying the MC simulation for thickness dependence of effective mobility, we found that the material thickness has a substantial impact on the μ_h^{eff} and consequently on the free charge collection efficiency in the MAPbBr₃ devices. Further, our results demonstrate that for studying the transport properties of OMHP devices such as assessment of drift mobility, lifetime, and mobility lifetime product the role of traps should be carefully considered.

This study is a pathfinder on parameters of trap affected charge dynamics in MAPbBr₃ perovskite. The overcoming of the demonstrated interplay between free charge and traps advance a new generation of OMHP materials and their optoelectronic applications.

Methods

Time of Flight spectroscopy

Time-of-Flight (ToF) method is based on measurement of the current response in a planar semiconductor device with an external stimulation (such as an alpha particle, electron, short light pulse, etc.). In our experimental setup, this external stimulus is an above bandgap laser pulse (laser-induced transient current technique, L-TCT). The optical pulse generates electron-hole pairs near the illuminated electrode. By applying an electric field, the electron-hole pairs are separated. Free holes drift towards the cathode and generate a current according to the Shockley-Ramo theorem. The anode immediately collects free electrons therefore only free holes drifting in the material generates Current waveforms (CWFs) signal. In these measurements, the CWFs is recorded by a synchronous triggering derived from the laser pulse. This set up results a much better signal to noise ratio as compare to un-triggered sources like alpha particles. Often the enhanced continuous DC biasing (tens of V) in an OMHP device results in dynamic degradation of the sample, which makes the reliable record of CWF impossible. To overcome this detrimental effect, we apply an a synchronized pulsed biasing. A light source with a photon energy of 2.7 eV (460 nm) is used to generate free carriers at the anode. The above-bandgap light pulse is preferably absorbed in less than 1 μ m thick layer below the contact electrode. A positive bias, U, is applied between the two electrodes to collect free charge carriers. The current signal is detected using an oscilloscope synchronized with laser and voltage pulses. Using such pulse photo-excitation

allows us an accumulation and averaging of multiple current waveforms resulting in a high signal to noise ratio. The additional description can be found in supplementary materials (Figures S4-S5).

Monte Carlo simulation

We use Monte Carlo calculation to simulate charge dynamics in MAPbBr₃ single crystal device. We developed 1D MC with the total number of particles, $N = 10^5$. The initial position x of the MC particle is generated according to Lambert-Beer law for light absorption. Our MC simulation also includes the diffusion of the carriers in addition to simulated drift process between two metal contacts. Each MC simulation step changes the state of the MC particle using random numbers according to probability given by trapping and detrapping time of particular trap level. We found parameters (trapping/detrapping time) of each trap in the band gap by fitting experimental ToF results with MC simulation and least square regression analysis. Current waveforms are calculated using Shockley-Ramo theorem. The detailed description of the method is given in supplementary materials (Figures S1-S2 and Equations S1-S6).

The effective mobility is a useful approximation of free charged carrier cloud movement. When free carriers drift in the material and interact with traps, the center of the charge cloud moves with an effective mobility rather than with microscopic one. This approximation relies on central limit theorem which states that when carriers undergo many trapping and detrapping events, a new equilibrium between traps and conduction band is established. The accuracy of the effective mobility depends on the number of trapping-detrapping events. If there is more than one trap level, the thermalization of traps starts with smallest detrapping time, after that the trap with larger detrapping time is thermalized and so on until all traps are thermalized. To reliably apply Monte Carlo simulation the number of trapping-detrapping events has to be several hundred in order to use the effective mobility approach. The typical error of effective mobility in this study is about 0.3%.

Single crystal MAPbBr₃ samples

Single crystal of MAPbBr₃ is grown from ultra-purity precursors. The sample geometry is $5 \times 5 \times 2 \text{ mm}^3$. Several samples showed the same ToF and MC simulation results, thus the results of one sample are presented in this work. Detail of single crystal growth can be found in our previous work^[23].

Acknowledgements

A. M., J. P., P.P, M. B., E. B., and R. G., thank the Institute of Physics of Charles University for providing necessary facilities to conduct this research. A. M., J. P., P.P, M. B., E. B., and R. G acknowledge financial support from the Grant Agency of the Czech Republic, Grant No. P102/19/11920S and the Grant Agency of Charles University, project No. 1234119. M.A. and B.D. acknowledge financial support from US Department of Homeland Security (grant # 2016-DN-077-ARI01).

References:

- [1] T. Tiedje, E. Yablonovitch, G. D. Cody, B. G. Brooks, *IEEE Trans. Electron Devices* **1984**, *31*, 711.
- [2] "Efficiency chart 2019," can be found under <https://www.nrel.gov/pv/assets/pdfs/best-research-cell-efficiencies.pdf>, **n.d.**
- [3] A. Kojima, K. Teshima, Y. Shirai, M. Tsutomu, *J. Am. Chem. Soc.* **2009**, *131*, 6050.
- [4] J. Yoon, H. Sung, G. Lee, W. Cho, N. Ahn, H. S. Jung, M. Choi, *Energy Environ. Sci.* **2017**, *10*, 337.
- [5] D. Yang, R. Yang, S. Priya, S. F. Liu, *Angew. Chemie Int. Ed.* **2019**, *58*, 4466.
- [6] J. Feng, X. Zhu, Z. Yang, X. Zhang, J. Niu, Z. Wang, S. Zuo, S. Priya, S. F. Liu, D. Yang, *Adv. Mater.* **2018**, *30*, 1801418.

- [7] Y. Hu, Y. Bai, B. Luo, S. Wang, H. Hu, P. Chen, M. Lyu, J. Shapter, A. Rowan, L. Wang, *Adv. Energy Mater.* **2019**, 1900872.
- [8] Y. Hu, Y. Bai, B. Luo, S. Wang, H. Hu, P. Chen, M. Lyu, J. Shapter, A. Rowan, L. Wang, *Adv. Energy Mater.* **2019**, 1900872.
- [9] S. Gharibzadeh, B. Abdollahi Nejand, M. Jakoby, T. Abzieher, D. Hauschild, S. Moghadamzadeh, J. A. Schwenzler, P. Brenner, R. Schmager, A. A. Haghighirad, L. Weinhardt, U. Lemmer, B. S. Richards, I. A. Howard, U. W. Paetzold, *Adv. Energy Mater.* **2019**, 9, 1803699.
- [10] S. Yun, Y. Qin, A. R. Uhl, N. Vlachopoulos, M. Yin, D. Li, X. Han, A. Hagfeldt, *Energy Environ. Sci.* **2018**, 11, 476.
- [11] G. E. Eperon, T. Leijtens, K. A. Bush, R. Prasanna, T. Green, J. T.-W. Wang, D. P. McMeekin, G. Volonakis, R. L. Milot, R. May, A. Palmstrom, D. J. Slotcavage, R. A. Belisle, J. B. Patel, E. S. Parrott, R. J. Sutton, W. Ma, F. Moghadam, B. Conings, A. Babayigit, H.-G. Boyen, S. Bent, F. Giustino, L. M. Herz, M. B. Johnston, M. D. McGehee, H. J. Snaith, *Science* **2016**, 354, 861.
- [12] J. H. Heo, S. H. Im, *Adv. Mater.* **2016**, 28, 5121.
- [13] M. Jošt, E. Köhnen, A. B. Morales-Vilches, B. Lipovšek, K. Jäger, B. Macco, A. Al-Ashouri, J. Krč, L. Korte, B. Rech, R. Schlatmann, M. Topič, B. Stannowski, S. Albrecht, *Energy Environ. Sci.* **2018**, 11, 3511.
- [14] K. T. Cho, S. Paek, G. Grancini, C. Roldán-Carmona, P. Gao, Y. Lee, M. K. Nazeeruddin, *Energy Environ. Sci.* **2017**, 10, 621.
- [15] S. S. Mali, C. S. Shim, C. K. Hong, *NPG Asia Mater.* **2015**, 7, e208.
- [16] R. Sheng, A. Ho-Baillie, S. Huang, S. Chen, X. Wen, X. Hao, M. A. Green, *J. Phys. Chem. C* **2015**, 119, 3545.
- [17] L. Zhang, X. Yang, Q. Jiang, P. Wang, Z. Yin, X. Zhang, H. Tan, Y. Yang, M. Wei, B. R. Sutherland, E. H. Sargent, J. You, *Nat. Commun.* **2017**, 8, 15640.
- [18] M. R. Leyden, L. Meng, Y. Jiang, L. K. Ono, L. Qiu, E. J. Juarez-Perez, C. Qin, C. Adachi, Y. Qi, *J. Phys. Chem. Lett.* **2017**, 8, 3193.
- [19] N. Pourdavoud, A. Mayer, M. Buchmüller, K. Brinkmann, T. Häger, T. Hu, R. Heiderhoff, I. Shutsko, P. Görrn, Y. Chen, H.-C. Scheer, T. Riedl, *Adv. Mater. Technol.* **2018**, 3, 1700253.
- [20] M. Ahmadi, T. Wu, B. Hu, *Adv. Mater.* **2017**, 29, 1605242.
- [21] H. Wei, D. DeSantis, W. Wei, Y. Deng, D. Guo, T. J. Savenije, L. Cao, J. Huang, *Nat. Mater.* **2017**, 16, 826.
- [22] H. Wei, Y. Fang, P. Mulligan, W. Chuirazzi, H.-H. Fang, C. Wang, B. R. Ecker, Y. Gao, M. A. Loi, L. Cao, J. Huang, *Nat. Photonics* **2016**, 10, 333.
- [23] J. T. Tisdale, T. Smith, J. R. Salasin, M. Ahmadi, N. Johnson, A. V. Ievlev, M. Koehler, C. J. Rawn, E. Lukosi, B. Hu, *CrystEngComm* **2018**, 20, 7818.
- [24] E. Lukosi, T. Smith, J. Tisdale, D. Hamm, C. Seal, B. Hu, M. Ahmadi, *Nucl. Instruments Methods Phys. Res. Sect. A Accel. Spectrometers, Detect. Assoc. Equip.* **2019**, 927, 401.
- [25] S. M. Sze, S. M., *New York, Wiley-Interscience, 1981. 878 p.* **1981**.
- [26] M. Grundmann, *The Physics of Semiconductors : An Introduction Including Devices and Nanophysics*, Springer, **2006**.
- [27] A. Musiienko, P. Moravec, R. Grill, P. Praus, I. Vasylchenko, J. Pekarek, J. Tisdale, K. Ridzonova, E. Belas, L. Landová, B. Hu, E. Lukosi, M. Ahmadi, *Energy Environ. Sci.* **2019**, 12, 1413.

- [28] A. Musiienko, R. Grill, P. Moravec, P. Fochuk, I. Vasylychenko, H. Elhadidy, L. Šedivý, *Phys. Rev. Appl.* **2018**, *10*, 014019.
- [29] Y. Bi, E. M. Hutter, Y. Fang, Q. Dong, J. Huang, T. J. Savenije, *J. Phys. Chem. Lett.* **2016**, *7*, 923.
- [30] A. A. B. Baloch, F. H. Alharbi, G. Grancini, M. I. Hossain, M. K. Nazeeruddin, N. Tabet, *J. Phys. Chem. C* **2018**, *122*, 26805.
- [31] Y. Chen, T. Wang, Z. Li, H. Li, T. Ye, C. Wetzel, H. Li, S.-F. Shi, *Sci. Rep.* **2018**, *8*, 16482.
- [32] F. Chen, C. Zhu, C. Xu, P. Fan, F. Qin, A. Gowri Manohari, J. Lu, Z. Shi, Q. Xu, A. Pan, *J. Mater. Chem. C* **2017**, *5*, 7739.
- [33] P. S. Whitfield, N. Herron, W. E. Guise, K. Page, Y. Q. Cheng, I. Milas, M. K. Crawford, *Sci. Rep.* **2016**, *6*, 35685.
- [34] I. Levine, O. G. Vera, M. Kulbak, D.-R. Ceratti, C. Rehmann, J. A. Márquez, S. Levchenko, T. Unold, G. Hodes, I. Balberg, D. Cahen, T. Dittrich, *ACS Energy Lett.* **2019**, *4*, 1150.
- [35] C. M. Sutter-Fella, D. W. Miller, Q. P. Ngo, E. T. Roe, F. M. Toma, I. D. Sharp, M. C. Lonergan, A. Javey, *ACS Energy Lett.* **2017**, *2*, 709.
- [36] A. Buin, R. Comin, J. Xu, A. H. Ip, E. H. Sargent, *Chem. Mater.* **2015**, *27*, 4405.
- [37] D. Shi, V. Adinolfi, R. Comin, M. Yuan, E. Alarousu, A. Buin, Y. Chen, S. Hoogland, A. Rothenberger, K. Katsiev, Y. Losovyj, X. Zhang, P. A. Dowben, O. F. Mohammed, E. H. Sargent, O. M. Bakr, *Science* **2015**, *347*, 519.
- [38] D. Meggiolaro, S. G. Motti, E. Mosconi, A. J. Barker, J. Ball, C. Andrea Riccardo Perini, F. Deschler, A. Petrozza, F. De Angelis, *Energy Environ. Sci.* **2018**, *11*, 702.
- [39] T. Leijtens, G. E. Eperon, A. J. Barker, G. Grancini, W. Zhang, J. M. Ball, A. R. S. Kandada, H. J. Snaith, A. Petrozza, *Energy Environ. Sci.* **2016**, *9*, 3472.
- [40] J. Chen, N.-G. Park, *Adv. Mater.* **2018**, 1803019.
- [41] M.-H. Du, *J. Phys. Chem. Lett.* **2015**, *6*, 1461.
- [42] A. Musiienko, R. Grill, J. Pekárek, E. Belas, P. Praus, J. Pipek, V. Dědič, H. Elhadidy, *Appl. Phys. Lett.* **2017**, *111*, 082103.
- [43] P. Praus, E. Belas, J. Bok, R. Grill, J. Pekarek, *IEEE Trans. Nucl. Sci.* **2016**, *63*, 246.
- [44] K. Suzuki, T. Sawada, S. Seto, *Phys. status solidi* **2016**, *13*, 656.
- [45] R. H. Bube, *Photoconductivity of Solids*, Wiley, New York, **1960**.
- [46] D. C. Hoesterey, G. M. Letson, *J. Phys. Chem. Solids* **1963**, *24*, 1609.
- [47] P. Calado, A. M. Telford, D. Bryant, X. Li, J. Nelson, B. C. O'Regan, P. R. F. Barnes, *Nat. Commun.* **2016**, *7*, 13831.
- [48] D. C. Hoesterey, G. M. Letson, *J. Phys. Chem. Solids* **1963**, *24*, 1609.
- [49] Q. Dong, Y. Fang, Y. Shao, P. Mulligan, J. Qiu, L. Cao, J. Huang, *Science (80-.)*. **2015**, *347*, 967.
- [50] Y. Hu, E. M. Hutter, P. Rieder, I. Grill, J. Hanisch, M. F. Aygüler, A. G. Hufnagel, M. Handloser, T. Bein, A. Hartschuh, K. Tvingstedt, V. Dyakonov, A. Baumann, T. J. Savenije, M. L. Petrus, P. Docampo, *Adv. Energy Mater.* **2018**, *8*, 1703057.
- [51] G. Ariño-Estrada, M. Chmeissani, G. de Lorenzo, M. Kolstein, C. Puigdengoles, J. García, E. Cabruja, *J. Instrum.* **2014**, *9*, C12032.
- [52] S. Tiwari, N. C. Greenham, *Opt. Quantum Electron.* **2009**, *41*, 69.
- [53] A. M. Barnett, J. E. Lees, D. J. Bassford, J. S. Ng, *Nucl. Instruments Methods Phys. Res. Sect. A Accel. Spectrometers, Detect. Assoc. Equip.* **2012**, *673*, 10.

- [54] G. Lioliou, A. M. Barnett, *Nucl. Instruments Methods Phys. Res. Sect. A Accel. Spectrometers, Detect. Assoc. Equip.* **2016**, 836, 37.
- [55] Y. Hu, E. M. Hutter, P. Rieder, I. Grill, J. Hanisch, M. F. Aygüler, A. G. Hufnagel, M. Handloser, T. Bein, A. Hartschuh, K. Tvingstedt, V. Dyakonov, A. Baumann, T. J. Savenije, M. L. Petrus, P. Docampo, *Adv. Energy Mater.* **2018**, 8, 1703057.